

# Analysis of the directionality on periodic materials

Nicolás Guarín-Zapata, Camilo Valencia, Juan Gomez  
Universidad EAFIT, Departamento de Ingeniería Civil, Medellín, Colombia

September 15, 2021

## Abstract

We present a method to visualize the directionality of periodic materials. This method takes as input dispersion (hyper-) surfaces obtained using a Bloch analysis and outputs a curve/surface with the bulk directionality encoded on it. Although the examples shown are in the context of elastodynamics the method can be used without need of consideration for the underlying physical phenomena.

**Keywords:** Periodic material, phononic crystal, dispersion relation, Bloch analysis, directionality, visualization.

## 1 Introduction

There is an increasing interest in the study and design of periodic materials across disciplines (Banerjee, 2011; Joannopoulos et al., 2008; Deymier, 2013). This interest is related to the appearance of unusual properties such as effective negative mass, negative refraction, negative Poisson equation, and acoustic/electromagnetic cloaking (Norris and Haberman, 2012; Hussein et al., 2014; Goldsberry and Haberman, 2018). Thus, there is a trend in designing microstructures aiming to control the bulk properties (Milton and Cherkaev, 1995; Norris and Nagy, 2011; Willis, 2016; Valencia et al., 2019b; Guarín-Zapata et al., 2019). Although direct numerical simulations, where the bulk of the material is considered and the complete microstructure is discretized are possible (Sigalas and Garcia, 2000), the most common approach is to take advantage of the periodicity of the material and model a single cell (Pennec et al., 2010; Hussein et al., 2014). This is achieved

using Bloch's theorem (Bloch, 1929). Bloch's theorem was originally used in solid-state physics (Brillouin, 2003; Kittel, 1996), but its use has been extended to electrodynamics (Joannopoulos et al., 2008), acoustics (Zhang and Liu, 2004; Deymier, 2013) and elastodynamics (Hussein et al., 2014; Valencia et al., 2019a; Guarín-Zapata et al., 2020).

Periodic materials are anisotropic because of discrete symmetries in their unit cells (Nye et al., 1985; Kittel, 1996; Moakher and Norris, 2006; Maurin et al., 2018). This anisotropy behavior translates into directionality in wave propagation, i.e., the speed of waves depends on the direction of propagation. So, if we want to study the propagation of waves in a periodic material, we are interested in characterizing this directionality. Although there have been some efforts in defining descriptors that quantify the anisotropy level of materials (Zener, 1948; Kanit et al., 2006; Ranganathan and Ostoja-Starzewski, 2008), they are not perfect because they reduce all the information to a single number and do not provide information about the preferred direction of propagation or symmetries present. Guarín-Zapata et al. (Guarín-Zapata et al., 2019) used a qualitative approach to compare anisotropy for different transversely isotropic materials and select them to tune the behavior of helicoidal composites. This was used for transversely isotropic materials, where the dispersion relations can be obtained analytically (Auld, 1973), and used to analyze a single layer of a composite. For heterogeneous materials and materials with other symmetries besides isotropy and transverse isotropy, this type of information is not available analytically and numerical simulations are required. Thus, a general tool to analyze the bulk anisotropy of materials is desired.

This work presents a method to compute a qualitative descriptor of material directionality for desired frequency ranges from dispersion (hyper-) surfaces. This starting point is a common output when using Bloch's theorem to analyze periodic materials. We start by describing some generalities of periodic materials and Bloch's theorem, which is commonly used to describe the bulk behavior using a single unit cell. Then, we describe the propagation of waves in anisotropic elastic materials in two and three dimensions. Following this section, we present the proposed method to analyze the directionality of periodic materials and present some tests for the method in analytically and numerically obtained dispersion relations. Although all the examples presented are from the field of elastodynamics this method applies to analyze the directionality for any material that uses dispersion (hyper-) surfaces as input.

## 2 Periodic materials

A periodic material is defined by the spatial repetition of a given motif in one, two, or three dimensions. The motifs refer to heterogeneities in the material properties at the microstructural level and can contain different materials, topologies, and shapes. For example, in the case of electromagnetic waves, we have *photonic crystals* and the periodicity of electric permittivity and magnetic permeability (Joannopoulos et al., 2008). For elastic waves, the term is *phononic crystals* and we have periodicity in the stiffness and mass density of the material (Deymier, 2013). These materials are completely described by a lattice and an elementary or unit cell. The lattice is defined by a set of base vectors, which allow the construction of the whole material applying successive translation operations (Brillouin, 2003). To study this type of material it is common to take advantage of the periodicity of the material properties and express the solution using Bloch's theorem (Brillouin, 2003).

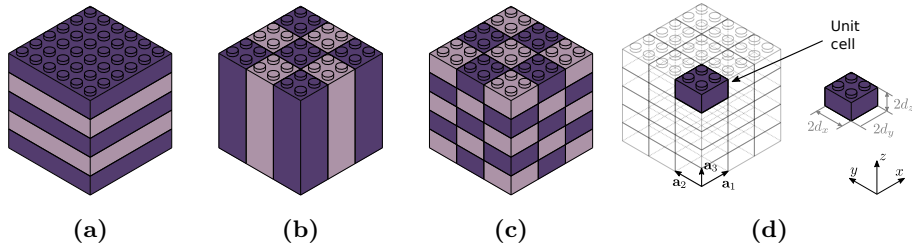


**Figure 1.** 3D material with different periodicities. Regardless of the space dimensionality its periodicity could be in (a) one (b) two or (c) three space dimensions. (d) The purple lego-brick defines the fundamental unit cell which allows construction or filling of space after applying translation operations according to the lattice vector  $\mathbf{a}$ .

### 2.1 Bloch's theorem

Let us consider a generalized wave equation of the form

$$\mathcal{L}\mathbf{u}(\mathbf{x}) = -\omega^2\mathbf{u}(\mathbf{x}), \quad (1)$$

where  $\mathcal{L}$  is a positive definite operator (Johnson, 2010; Reddy, 1991),  $\mathbf{u}$  is the field of interest, and  $\omega$  is the angular frequency. Bloch's theorem establishes

that solutions to (1) are of the form

$$\mathbf{u}(\mathbf{x}) = \mathbf{w}(\mathbf{x})e^{i\mathbf{k}\cdot\mathbf{x}}, \quad (2)$$

where  $\mathbf{w}(\mathbf{x})$  is a function with the same periodicity of the material. Opposite sides of the unit cell and separated by a vector  $\mathbf{a}$  and, as a consequence,

$$\mathbf{u}(\mathbf{x} + \mathbf{a}) = \mathbf{u}(\mathbf{x})e^{i\mathbf{k}\cdot\mathbf{a}}.$$

Where  $\mathbf{u}(\mathbf{x} + \mathbf{a})$  and  $\mathbf{u}(\mathbf{x})$  give the field at  $\mathbf{x} + \mathbf{a}$  and  $\mathbf{x}$ , while  $\mathbf{a} = \mathbf{a}_1 n_1 + \mathbf{a}_2 n_2 + \mathbf{a}_3 n_3$  is the lattice translation vector shown in Figure 1(d). The term  $e^{i\mathbf{k}\cdot\mathbf{a}}$  represents a phase shift between opposite sides of the unit cell. This relationship between opposite sides of the fundamental cell stated in the theorem through the boundary terms permits the characterization of the fundamental properties of the material with the analysis of a single cell.

Computationally, equation (1) is commonly translated to a generalized eigenvalue problem through a numerical method such as the Finite Element Method. And we end up with a system of the form

$$[K]\{\mathbf{U}\} = \omega^2[M]\{\mathbf{U}\},$$

where  $[K]$  is the stiffness matrix and  $[M]$  is the mass matrix. Bloch's theorem can be applied through boundary conditions imposed strongly by including directly the phase shifts at the element level or performing row and column operations in these matrices (Valencia et al., 2019a); or weakly imposing them through Lagrange multipliers or penalty methods (Michel et al., 1999; Sukumar and Pask, 2009). After this process, we end up with the following system

$$[K_R(\mathbf{k})]\{\mathbf{U}_R\} = \omega^2[M_R(\mathbf{k})]\{\mathbf{U}_R\},$$

where  $\mathbf{k}$  is the wave vector which is progressively assigned successive values, in such a way that the first Brillouin zone is fully covered. Each evaluation for a particular wave vector and the solution of the related eigenvalue problem yields tuples of the form  $(\mathbf{k}, \omega_n)$  representing a plane wave propagating at frequency  $\omega_n$ . The subindex  $n$  refers to the  $n$ th eigenvalue computed for the input wave vector  $\mathbf{k}$ , this is depicted in Figure 2.

Having multiple dispersion surfaces is common for problems in electrodynamics or elastodynamics (Joannopoulos et al., 2008; Banerjee, 2011). In

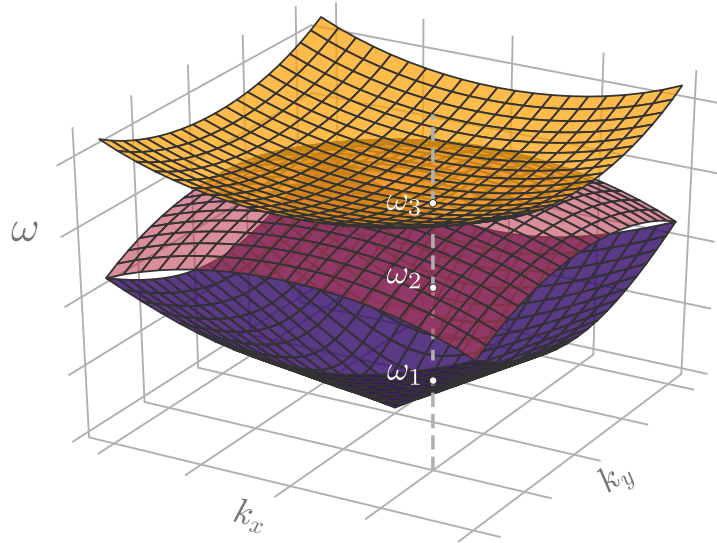


**Figure 2.** Schematic depicting the multiple branches obtained in a Bloch analysis. For a single point in the wavevector space there are multiple values for the frequency.

In the case of homogeneous materials we have two transverse modes for electromagnetic waves and two transverse modes plus a longitudinal one for elastic waves. Nevertheless, Bloch analysis introduces an additional complication since the computations are done in the first Brillouin zone. Here, wavevectors are determined up to an additive constant that is written in terms of the lattice vectors

$$\mathbf{a}_1 n_1 + \mathbf{a}_2 n_2 + \mathbf{a}_3 n_3 \quad \forall n_1, n_2, n_3 \in \mathbb{Z}.$$

This means that  $\mathbf{k}$  and  $\mathbf{k} + \mathbf{a}_1 n_1 + \mathbf{a}_2 n_2 + \mathbf{a}_3 n_3$ , are assigned to the same point in the first Brillouin zone. Figure 3 illustrates this effect for the first three dispersion surfaces for a homogeneous material.

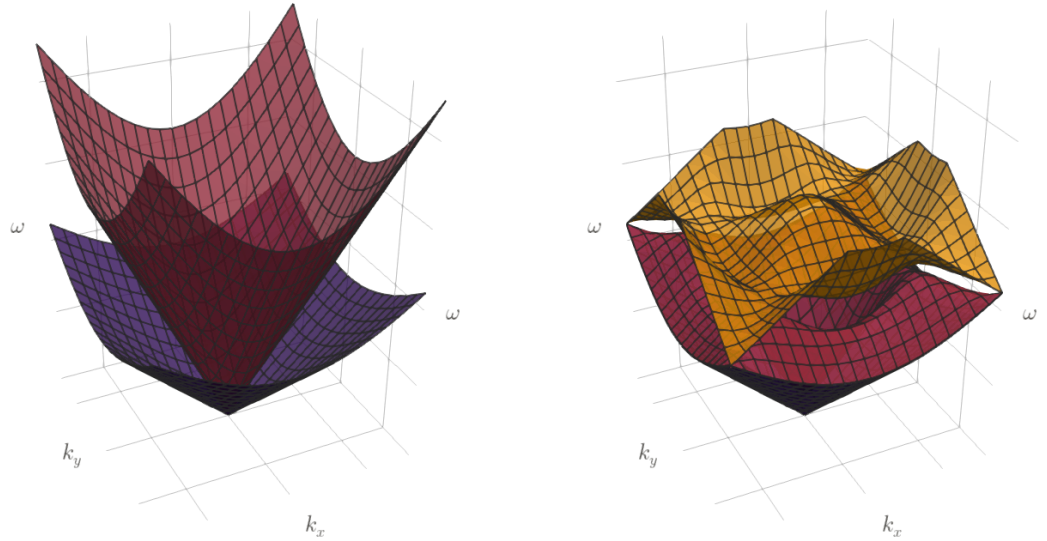


**Figure 3.** Comparison of the dispersion surfaces for a homogeneous material computed with the classical expression (left) with the dispersion surfaces obtained using Bloch analysis (right). Here we are showing the first three branches.

As shown in Figure 3, when using Bloch analysis we obtain dispersion surfaces ordered by frequency. This might lead to conclude that materials are anisotropic when they are not, as shown in Figure 4. For low wavenumbers, we can see that the material is isotropic/anisotropic when looking at the first mode. Nevertheless, this is not the case when looking at the second and third modes. Furthermore, anisotropy in one material might be more pronounced in one propagation mode than in others.

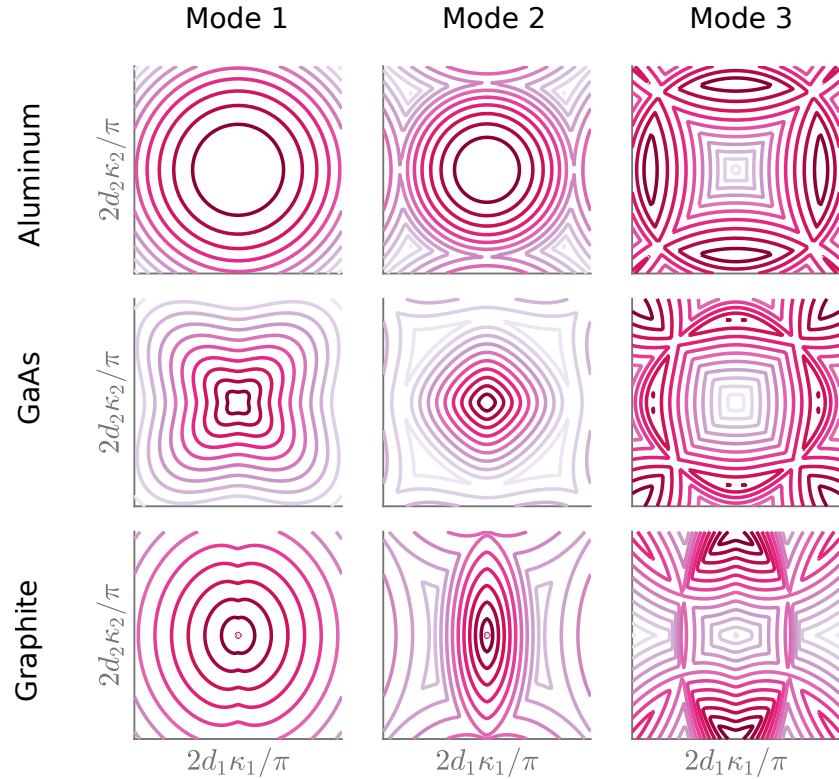


**Figure 4.** Comparison of the contours of iso-frequency for the first three dispersion modes for isotropic, cubic and orthotropic materials. **(Top)** Contours for aluminum, an isotropic example. **(Middle)** Contours for GaAs, a cubic example. **(Bottom)** Contours for graphite, an orthotropic example.

This apparent anisotropy is more difficult to analyze if we consider wave propagation in three dimensions instead of two, as can be seen in Figure 5.

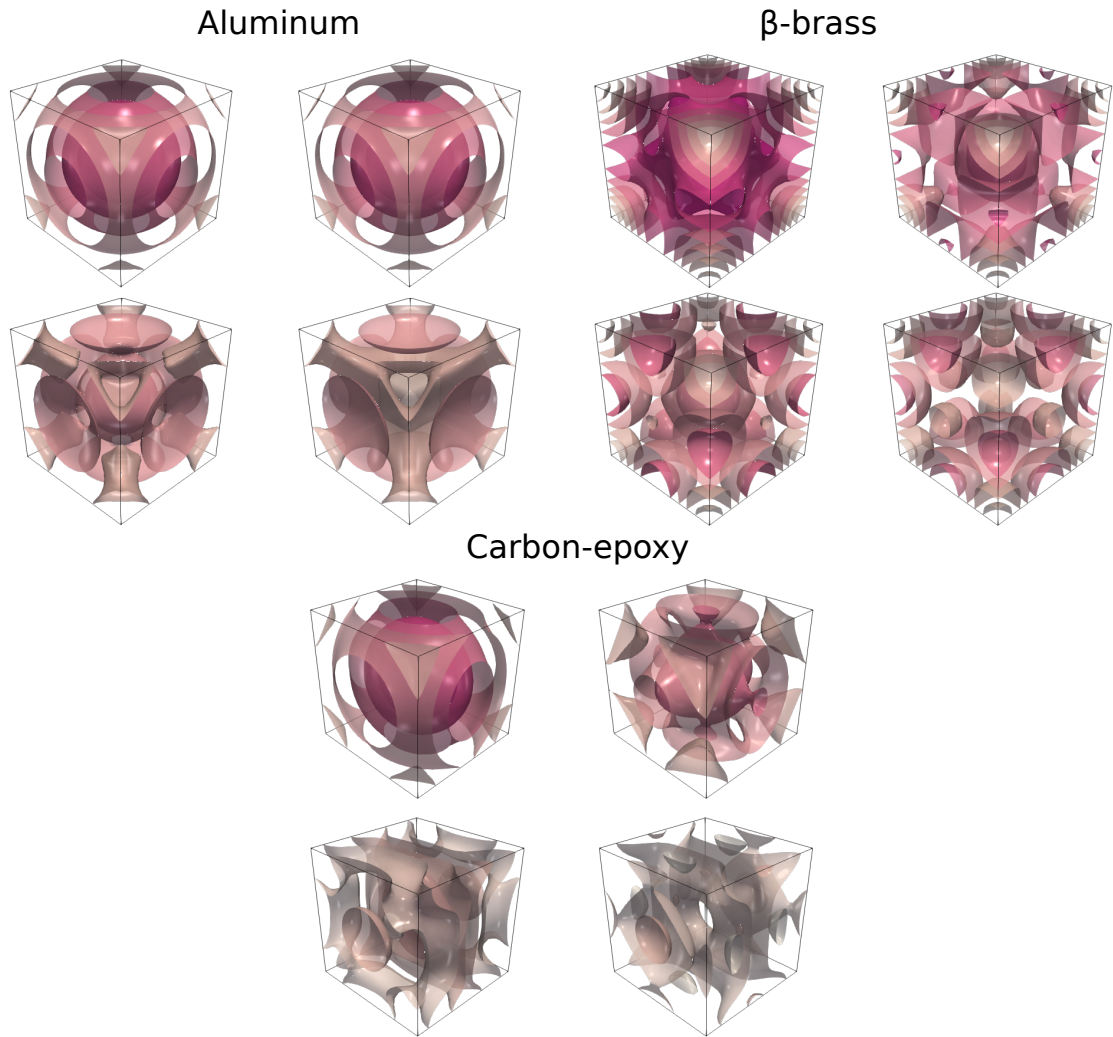


**Figure 5.** Comparison of the the surface of iso-frequency for the four three dispersion modes for isotropic, cubic and transverse isotropic materials.

### 3 Elastic wave propagation in anisotropic media

As mentioned before, periodic materials are inherently anisotropic due to their microstructure. Their *level* of anisotropy obeys the symmetries present.

Following, in this section we describe the propagation of waves for elastic solids of general anisotropy.

Let us consider a wave that propagates in a solid. In this case, the conservation of density of momentum in the absence of body forces is written as

$$\sigma_{ij,i} = \rho \frac{\partial^2 u_i}{\partial t^2},$$

with  $\sigma_{ij}$  the stress tensor,  $u_i$  the displacement vector, and  $\rho$  the mass density. In the case of a linear elastic material, Hooke's law is given by

$$\sigma_{ij} = c_{ijkl} u_{k,l},$$

where  $c_{ijkl}$  is the stiffness tensor that can have up to 21 constants in the case of general anisotropy.

If we assume a plane-wave solution of the form

$$u_j = U_j e^{ik(n_m x_m - v_p t)};$$

where  $k = |\mathbf{k}|$  is the wavenumber,  $n_m$  is a unit vector in the direction of  $\mathbf{k}$ , and  $v_p$  is the phase speed; we end up with the Christoffel wave equation ([Buchwald, 1959](#); [Auld, 1973](#); [Carcione, 2007](#)):

$$[\Gamma_{ij} - \rho v_p^2 \delta_{ij}] U_j = 0,$$

where  $\Gamma_{ij} = c_{ijkl} n_k n_l$  is the Christoffel stiffness tensor or acoustic tensor, and  $\delta_{ij}$  is the Kronecker delta. This is an eigenvalue problem, where the eigenvalues  $\rho v_p^2$  gives the phase speeds for the material. The corresponding characteristic polynomial is

$$\det[\Gamma_{ij} - \rho v_p^2 \delta_{ij}] = 0. \quad (3)$$

From (3) we conclude that there are three propagating waves, each one with a different polarization. These directions are orthogonal since  $\Gamma_{ij}$  is symmetric. From the three polarizations, we have two quasi-transverse (qS) waves and one quasi-longitudinal (qP) wave. Where the prefix *quasi* implies that two of the modes are close to orthogonal to the wavevector and the other is close to parallel to it. As we can see, the value of  $\Gamma_{ij}$  depends on the direction of propagation implying that the phase speed depends on the direction of the wave (see Figure 6). We can rewrite (3) as

$$\Omega(\omega, \mathbf{k}) = \det \left[ \Gamma_{ij} - \rho \frac{\omega^2}{\|\mathbf{k}\|^2} \delta_{ij} \right], \quad (4)$$

taking into account that the phase speed is defined as  $v_p^2 = \omega^2/\|\mathbf{k}\|^2$ . The group velocity is defined as (Auld, 1973)

$$\mathbf{v}_g = \frac{\nabla_{\mathbf{k}}\Omega}{\partial\Omega/\partial\omega}, \quad (5)$$

and for lossless media it represents the direction of energy flow.

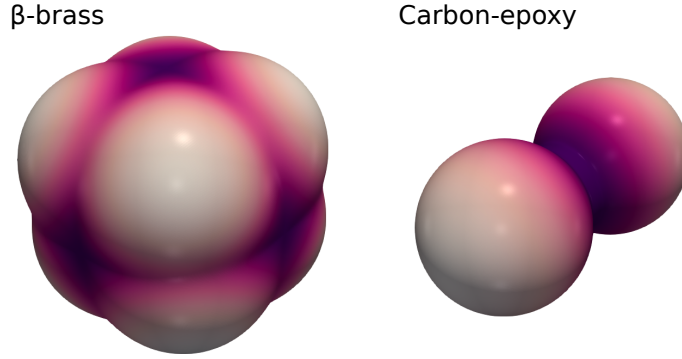


**Figure 6.** Comparison of the the surface of relative phase speed for the quasi-longitudinal (qP) mode for cubic and transverse isotropic materials.

## 4 Evaluation of directionality

Elastic anisotropy plays a role in different applications such as metallurgy (Zener, 1948), geophysics (Thomsen, 1986), wave propagation in composites (Guarín-Zapata et al., 2019), and metamaterials (Casadei and Rimoli, 2013), among others. Thus, for a particular application, one might need a material with more or less anisotropy, and the question of how anisotropic different materials are arises naturally.

### 4.1 Some existing measures of anisotropy

One of the first measures of anisotropy was the Zener ratio (Zener, 1948) which is defined for cubic materials and is written as

$$a_r = \frac{2C_{44}}{C_{11} - C_{12}} = \frac{C_{44}}{C_{66}}.$$

From an intuitive perspective, it is defined as the ratio between the classical shear modulus and the *new one* that appears in cubic materials. The Zener ratio is one for isotropic materials. One extension of the Zener ratio for materials with more general anisotropy replaces the elastic coefficients by averages while retaining the form of the original ratio ([Kanit et al., 2006](#))

$$a_{\text{gen}} = \frac{2Y_{44}}{Y_{11} - Y_{12}},$$

with

$$Y_{11} = \frac{C_{11} + C_{22} + C_{33}}{3}, Y_{12} = \frac{C_{12} + C_{23} + C_{13}}{3}, Y_{44} = \frac{C_{44} + C_{55} + C_{66}}{3}.$$

There are other proposed metrics for measuring anisotropy such as the ratio of the maximum and minimum phase speed for the quasi-transverse modes ([Ledbetter and Migliori, 2006](#)) or the norm of the projection to the closest isotropic tensor ([Carcione, 2007](#)). [Ranganathan and Ostoja-Starzewski](#) compute some of these metrics for several crystals and compare them with a new metric termed universal anisotropy index (UAI). Although these metrics seem to be usable for general anisotropic materials they were conceived with homogeneous materials in mind.

Regarding the anisotropy of composites, it is common to present the directionality as group velocity polar histograms based on iso-frequency contours ([Ruzzene and Scarpa, 2005; Ruzzene et al., 2003](#)). Furthermore, [Casadei and Rimoli](#) computed an anisotropy index considering each propagation mode separately. This measure is, essentially, the standard deviation for each wave propagation mode. The main drawback with these approaches is that they considered just the first two or three modes of propagation, that is, low frequencies. Since phononic crystals can present dispersion it is expected that the anisotropy (directionality) depends on the frequency.

## 4.2 Method for directionality

[Valencia et al.](#) proposed a method to characterize the directionality of phononic crystals that considers the contribution of multiple modes, not just the low-frequency ones as in previous works ([Ruzzene and Scarpa, 2005; Ruzzene et al., 2003](#)). Thus, the approach allows a more complete description of the directional response in a material and is valid in the low and

high-frequency regimes. They defined the wave propagation directionality,  $D$ , as

$$D = \sum_{\substack{i \\ e>tol}} d_i(\theta), \quad d_i(\theta) = C(\nabla M_i) \quad (6)$$

where  $M_i$  is the  $i$ th mode in the dispersion relation,  $\nabla M_i$  is its gradient with respect to the wavevector  $\mathbf{k}$ ,  $tol$  is a predefined tolerance,  $\theta = [0, 2\pi]$  is the angle defining the propagation direction. In this definition, the operator  $C$  associates each vector to its direction ( $\theta$ ) and adds it to the previous vector sharing the same direction. Consequently,  $d_i = C(\nabla M_i)$  corresponds to a weighted polar histogram representing the distribution of group velocity for mode  $M_i$  in any propagation direction. The weight is given by the number of times a particular direction appears in the (discrete) dispersion relations. Thus, the method can be summarized as:

- Start from the frequency surface and compute the gradient to obtain group velocities.
- Sort the (discrete) gradient by angle and add their magnitudes when they share the angle.

These steps are depicted in Figure 7.

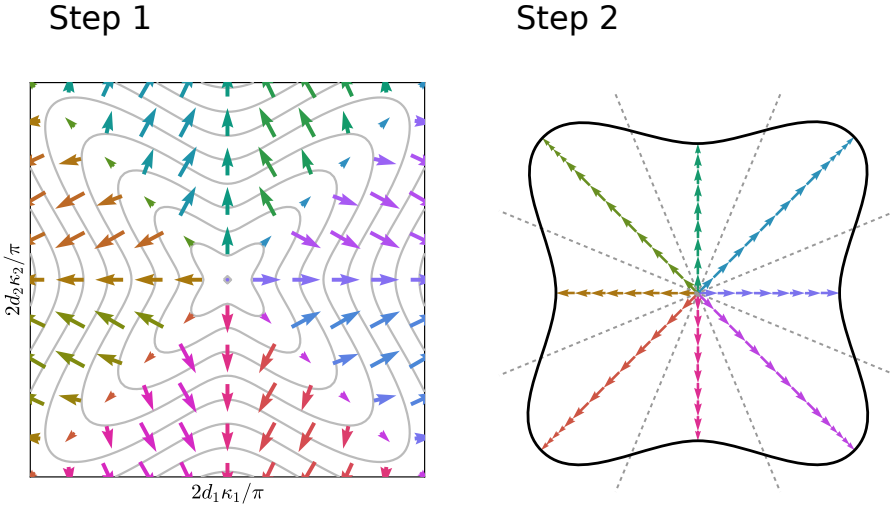


**Figure 7.** In **Step 1** we compute the gradient of the the  $i$ th mode of the dispersion curve. Then, in **Step 2** the group velocity vector are rearranged according to their direction and added. The resulting envelope curve represents the directionality for that mode.

One problem with this method is that it is considering group velocity vectors for regions with wavevector of different magnitudes. For example, when considering a square unit cell it will include more vectors associated to directions  $(1, 1)$ ,  $(-1, 1)$ ,  $(-1, -1)$  and  $(1, -1)$ . This makes the method depends on the shape of the unit cell chosen. Our proposed improvement is to average vectors instead of accumulating them. This is similar to restrict the analysis to wavevectors enclosed by a sphere with constant wavevector magnitude—in solid state physics states enclosed by a constant-energy surface are considered to compute the density of states (Kittel, 1996). As an example, let us compare the computed directionality for the first dispersion surface as shown in Figure 8.

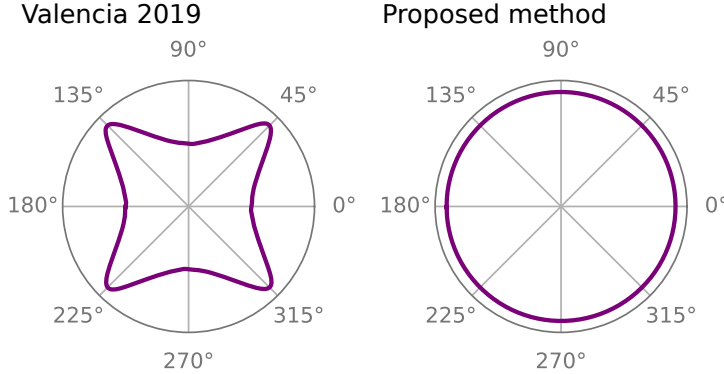


**Figure 8.** Comparison of the directionality computed using (**left**) Valencia et al. (2019b) method and (**right**) our approach.

Thus, the modified method can be summarized as:

- Start from the frequency surface and compute the gradient to obtain group velocities.
- Sort the (discrete) gradient by angle and average their magnitudes when they share the angle.

One natural question that arises after is how to extend the method to three dimensions. One difference when going from two to three dimensions is that there does not exist a uniform partition of the sphere. For instance, if the spherical coordinates parameterization is used there is a higher density of polygons in the poles. This is expected since the area differential in spherical coordinates is given by  $dA = r \sin \theta d\varphi d\theta$ , where  $\theta$  is the zenithal angle and  $\varphi$  the azimuthal angle (Arfken et al., 2005). To avoid this problem we used a triangulated mesh for the sphere that is close to uniform (Schlömer, 2020). Figure 9 provides a comparison of two meshes.

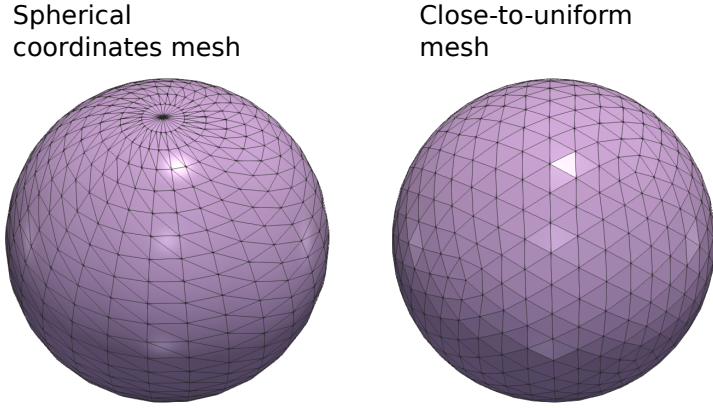


**Figure 9.** Comparison of a mesh of a sphere using a mesh that follows spherical coordinates and a close-to-uniform mesh. Notice the higher density of element in the pole of the left mesh.

Another difference between two and three dimensions is the absence of a *natural* order for the points<sup>1</sup>. To solve this problem we computed the spherical angles for each point in the sphere and created a k-D tree ([Scopatz and Huff, 2015](#); [Virtanen et al., 2020](#)). Then, at the moment of evaluating the direction of each group velocity vector, we made a nearest-neighbor search for its angles  $(\theta, \varphi)$  to assign the vector to a point on the sphere as was done in the two-dimensional case.

## 5 Results

To test the method, we computed the directionality for materials with different symmetry classes in two and three dimensions. First, we test the method using homogeneous materials that allow to us (semi) analytically obtain the dispersion relations and then we try it with results obtained using the finite element method for a micropolar elastic material. That also shows that the method does not depend on the equations being analyzed and only needs as input the dispersion relations.

---

<sup>1</sup>The preimage of the circle (1D) is an ordered set, that is, an interval—that follows the order of the real numbers. We cannot define this relation directly for the preimage of a sphere (2D).

## 5.1 Results for analytic dispersion relations

We want to solve the determinant in (4) for  $\omega$  to determine the dispersion relations. We rewrite the equation for completeness,

$$\Omega(\omega, \mathbf{k}) = \det \left[ \Gamma_{ij} - \rho \frac{\omega^2}{\|\mathbf{k}\|^2} \delta_{ij} \right] = 0.$$

This corresponds to solving a third-degree polynomial equation for each wavenumber  $\mathbf{k}$  (see the appendix at the end of this chapter for explicit forms of these equations). Then, for homogeneous materials, these relations can be solved semi-analytically and can be written as

$$\omega \equiv \omega(\mathbf{k}).$$

On the other hand, when these relationships are obtained from Bloch's theorem the dispersion relationships also contain information from different Brillouin zones leading to relations of the form

$$\omega_{m_1, m_1} \equiv \omega(\mathbf{k}_{m_1, m_1}), \quad (7)$$

in two dimensions, where the subscripts  $m_1, m_2$  correspond to integer numbers referring to waves coming from adjacent Brillouin zones. In the case of three dimensions the relations are of the form

$$\omega_{m_1, m_2, m_3} \equiv \omega(\mathbf{k}_{m_1, m_2, m_3}). \quad (8)$$

In the case of a square/cube unit cell with side  $d$ , we have the following generalized definition of the wavevector (Langlet, 1993):

$$\begin{aligned} \mathbf{k}_{m_1, m_2} &= \left( k_x + \frac{m_1 \pi}{d}, k_y + \frac{m_2 \pi}{d} \right), \\ \mathbf{k}_{m_1, m_2, m_3} &= \left( k_x + \frac{m_1 \pi}{d}, k_y + \frac{m_2 \pi}{d}, k_z + \frac{m_3 \pi}{d} \right), \end{aligned}$$

where  $k_x$ ,  $k_y$ , and  $k_z$  are the components of the wave vector.

Figure 10 presents a comparison of directionality for a periodic material with a square unit cell for aluminum (isotropic), GaAs (cubic) and Graphite (orthotropic). We can see that the directionality curves present the same symmetries than the material class in each case (see the appendix at the end for the material properties). The curve corresponding to the isotropic material is (almost) symmetric with respect to any rotation in the plane. In

the case of the cubic material, the curve remains the same after rotations of  $90^\circ$ . Finally, for the orthotropic material we can see a two planes of symmetry corresponding to the  $x$  and  $y$  axes.

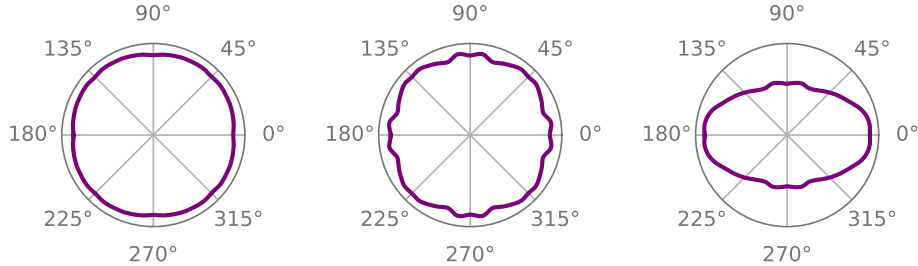


**Figure 10.** Comparison of directionality for a periodic material with a square unit cell for isotropic, cubic and orthotropic materials. (**Left**) Directionality for aluminum, an isotropic example. (**Center**) Directionality for GaAs, a cubic example. (**Right**) Directionality for graphite, an orthotropic example.

Figure 11 presents a comparison of directionality for a periodic material with a for  $\beta$ -brass (cubic) and cadmium (transverse isotropic). For the cubic material figure 11 presents a top view and an isometric view of the surface, the frontal and lateral views are omitted since it presents a symmetry with respect to rotations of  $90^\circ$ . In the case of the transverse isotropic material a third-angle projection plus the isometric view are presented. We can see that the directionality surfaces present the same symmetries as the material class in each case, in particular, the surface is (almost) symmetric with respect to the  $z$ -axis (see the appendix at the end for the material properties used).

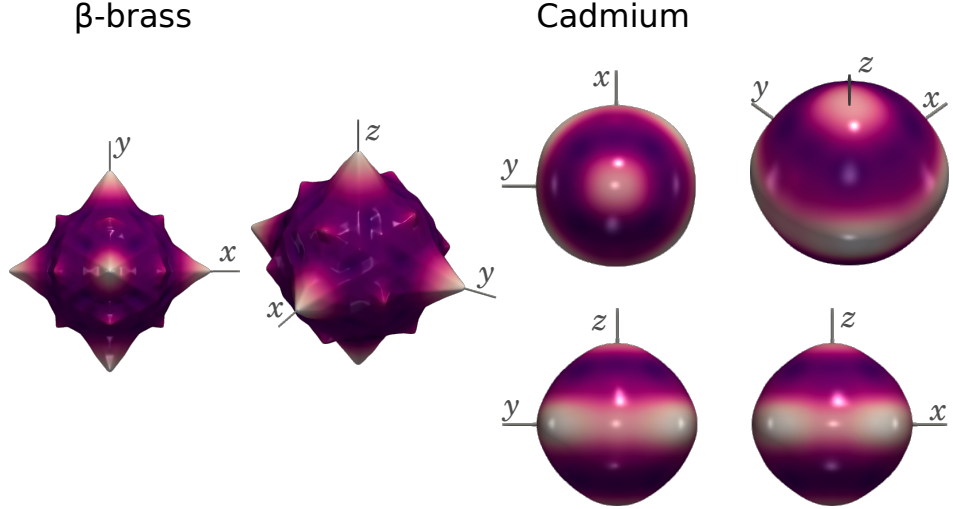


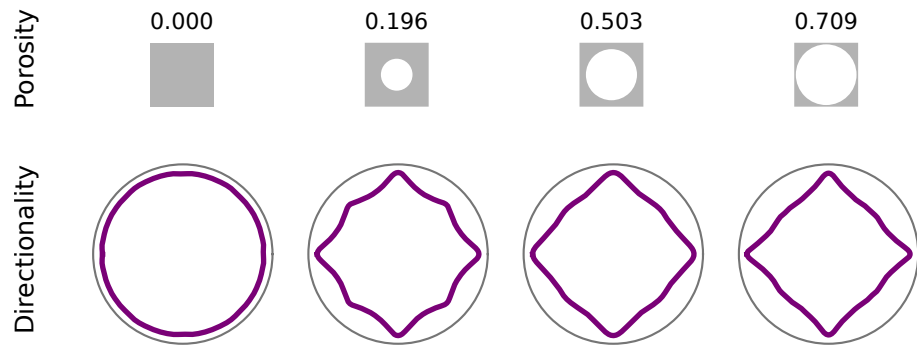
**Figure 11.** Comparison of the directionality surfaces for (**Left**)  $\beta$ -brass (**Right**) and cadmium.

## 5.2 Results for numerically-obtained dispersion relations

As a final result, we computed the directionality curves for cellular materials with circular pores. We changed the diameter of the pore while the size of the cell is kept fixed. The material used is a micropolar one with the following properties ([Guarín-Zapata et al., 2020](#)):

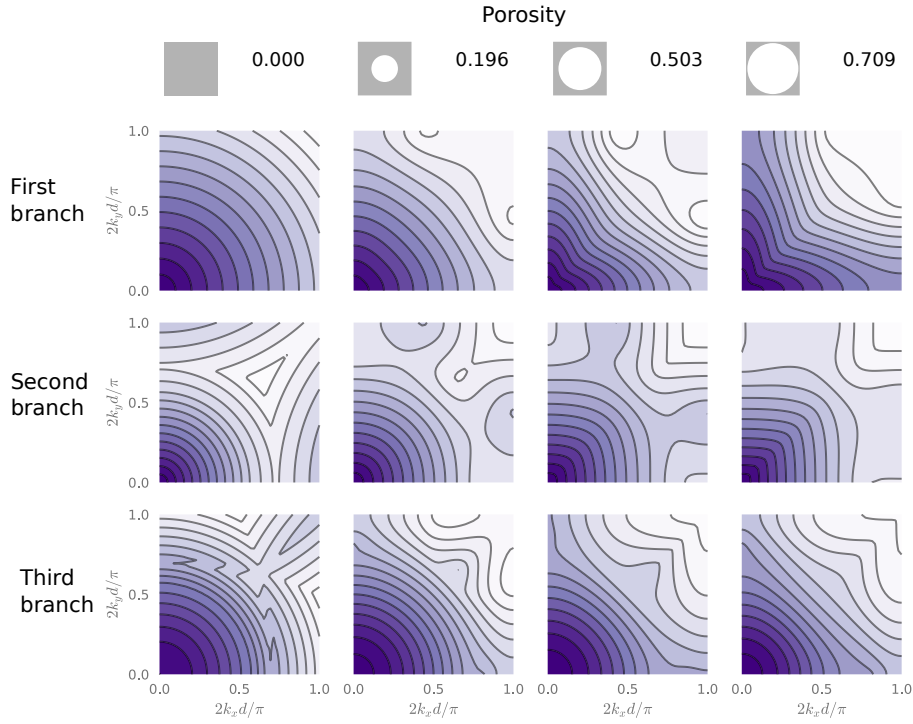
$$\begin{aligned} \rho &= 2770 \text{ kg/m}^3, & \lambda &= 5.12 \times 10^{10} \text{ Pa}, \\ \mu &= 2.76 \times 10^{10} \text{ Pa}, & \alpha &= 3.07 \times 10^9 \text{ Pa}, \\ \gamma + \epsilon &= 7.66 \times 10^{10} \text{ N}, & J &= 306.5 \text{ kg/m}. \end{aligned}$$

Figure 12 presents the computed directionality curves for increasing porosity values, namely: 0.000, 0.196, 0.503 and 0.709. A porosity of 0.0 represents a homogeneous material, used as a reference in this case. As expected, the directionality of the material increases with porosity, and the higher values for the averaged group speed happens along the  $x$  and  $y$  axes where we have continuous paths for the wave to propagate ([Valencia et al., 2019b](#)). Notice that the resulting curves are symmetric with respect to rotations of  $90^\circ$ . The same symmetry group can be seen in the unit cell.



**Figure 12.** Directionality curves for a cellular material with increasing porosity.

For comparison, we present the isofrequency contours for the first three branches of the dispersion relations for this material in Figure 13 ([Guarín-Zapata et al., 2020](#)).



**Figure 13.** Curves of isofrequency for a cellular material with increasing porosity for the first three branches. This are the plots usually used to analyze directionality in periodic materials. Originally published by ([Guarín-Zapata et al., 2020](#)).

## 6 Conclusions

We presented a method to visualize the directionality of waves in periodic materials modifying the work of [Valencia et al.](#) and extending it to the three-dimensional case. This method takes as input dispersion (hyper-) surfaces obtained using a Bloch analysis and outputs a curve/surface with the bulk directionality encoded on it. As such, it can be used for dispersion curves obtained in different physical contexts such as elastodynamics of electrodynamics. The approach used in this work does not separate modes  $M_i$  and wave types; instead, it deals with several modes at once allowing to present the directionality for a broadband frequency range and not just the low-frequency limit, as is common. Our approach provides a qualitative tool that is useful to describe the global behavior of waves when propagating

through the analyzed material; it is intended to be used as a complement to dispersion curves and surfaces.

## A Explicit form for the Christoffel equations

### A.1 Three dimensions

For a triclinic material with a stiffness tensor given by

$$[C] = \begin{bmatrix} C_{11} & C_{12} & C_{13} & C_{14} & C_{15} & C_{16} \\ C_{12} & C_{22} & C_{23} & C_{24} & C_{25} & C_{26} \\ C_{13} & C_{23} & C_{33} & C_{34} & C_{35} & C_{36} \\ C_{14} & C_{24} & C_{34} & C_{44} & C_{45} & C_{46} \\ C_{15} & C_{25} & C_{35} & C_{45} & C_{55} & C_{56} \\ C_{16} & C_{26} & C_{36} & C_{46} & C_{56} & C_{66} \end{bmatrix},$$

in Voigt notation, a density  $\rho$  and a wavevector  $\mathbf{k}$ , the equation that need to be solved is ([Auld, 1973](#))

$$\det \left( \|\mathbf{k}\|^2 \begin{bmatrix} \alpha & \delta & \varepsilon \\ \delta & \beta & \xi \\ \varepsilon & \xi & \gamma \end{bmatrix} \begin{bmatrix} u_1 \\ u_2 \\ u_3 \end{bmatrix} - \rho\omega^2 \begin{bmatrix} 1 & 0 & 0 \\ 0 & 1 & 0 \\ 0 & 0 & 1 \end{bmatrix} \begin{bmatrix} u_1 \\ u_2 \\ u_3 \end{bmatrix} \right) = 0, \quad (9)$$

with

$$\begin{aligned} \alpha &= C_{11}n_1^2 + C_{66}n_2^2 + C_{55}n_3^2 + 2C_{56}n_1n_3 + 2C_{15}n_3n_1 + 2C_{16}n_1n_2, \\ \beta &= C_{66}n_1^2 + C_{22}n_2^2 + C_{44}n_3^2 + 2C_{24}n_2n_3 + 2C_{46}n_3n_1 + 2C_{26}n_1n_2, \\ \gamma &= C_{55}n_1^2 + C_{44}n_2^2 + C_{33}n_3^2 + 2C_{34}n_2n_3 + 2C_{35}n_3n_1 + 2C_{45}n_1n_2, \\ \delta &= C_{16}n_1^2 + C_{26}n_2^2 + C_{33}n_3^2 + (C_{46} + C_{25})n_2n_3 + (C_{14} + C_{56})n_3n_1 \\ &\quad + (C_{12} + C_{66})n_1n_2, \\ \varepsilon &= C_{15}n_1^2 + C_{46}n_2^2 + C_{35}n_3^2 + (C_{45} + C_{36})n_2n_3 + (C_{13} + C_{55})n_2n_1 \\ &\quad + (C_{14} + C_{56})n_1n_2, \\ \zeta &= C_{56}n_1^2 + C_{24}n_2^2 + C_{34}n_3^2 + (C_{44} + C_{23})n_2n_3 + (C_{36} + C_{45})n_3n_1 \\ &\quad + (C_{25} + C_{46})n_1n_2, \end{aligned}$$

where  $\hat{\mathbf{n}} = (n_1, n_2, n_3) = \frac{\mathbf{k}}{\|\mathbf{k}\|}$ .

In the case of orthotropic materials aligned with the coordinate system these expressions can be simplified to

$$\begin{aligned}\alpha &= C_{11}n_1^2 + C_{66}n_2^2 + C_{55}n_3^2, \\ \beta &= C_{66}n_1^2 + C_{22}n_2^2 + C_{44}n_3^2, \\ \gamma &= C_{55}n_1^2 + C_{44}n_2^2 + C_{33}n_3^2, \\ \delta &= (C_{12} + C_{66})n_1n_2, \\ \varepsilon &= (C_{13} + C_{55})n_3n_1, \\ \zeta &= (C_{44} + C_{23})n_2n_3,\end{aligned}$$

this can be further simplified for cubic materials.

$$\begin{aligned}\alpha &= C_{11}n_1^2 + C_{44}(1 - n_1^2), \\ \beta &= C_{11}n_2^2 + C_{44}(1 - n_2^2), \\ \gamma &= C_{11}n_3^2 + C_{44}(1 - n_3^2), \\ \delta &= (C_{12} + C_{44})n_1n_2, \\ \varepsilon &= (C_{12} + C_{44})n_3n_1, \\ \zeta &= (C_{12} + C_{44})n_2n_3.\end{aligned}$$

For materials with transverse isotropic symmetry the equations can be solved analytically ([Carcione, 2007](#)). For a wave propagating in the plane 1-3, and taking  $n_2 = 0$ , we have

$$\begin{aligned}\omega_{qP}^2 &= \frac{\|\mathbf{k}\|^2(C_{11}n_1^2 + C_{33}n_3^2 + C_{55} + \sqrt{M})}{2\rho}, \\ \omega_{qS}^2 &= \frac{\|\mathbf{k}\|^2(C_{11}n_1^2 + C_{33}n_3^2 + C_{55} - \sqrt{M})}{2\rho}, \\ \omega_S^2 &= \frac{\|\mathbf{k}\|^2(C_{66}n_1^2 + C_{55}n_3^2)}{\rho}, \\ M &= [(C_{11} - C_{55})n_1^2 + (C_{55} - C_{33})n_3^2]^2 + 4[(C_{13} + C_{55})^2n_1n_3]^2.\end{aligned}$$

## A.2 Two dimensions

In the case of a monoclinic material we could align the symmetry plane to obtain the following two-dimensional problem

$$\det \left( \|\mathbf{k}\|^2 \begin{bmatrix} \alpha & \delta \\ \delta & \beta \end{bmatrix} - \rho\omega^2 \begin{bmatrix} 1 & 0 \\ 0 & 1 \end{bmatrix} \right) = 0,$$

that can be solved analytically as

$$\omega^2 = \frac{\|\mathbf{k}\|^2}{2\rho} [\alpha + \beta \pm \sqrt{(\alpha - \beta)^2 + 4\delta^2}]$$

with

$$\begin{aligned}\alpha &= C_{11}n_1^2 + C_{66}n_2^2 + 2C_{16}n_1n_2, \\ \beta &= C_{66}n_1^2 + C_{22}n_2^2 + 2C_{26}n_1n_2, \\ \delta &= C_{16}n_1^2 + C_{26}n_2^2 + (C_{12} + C_{66})n_1n_2,\end{aligned}$$

that reduces to

$$\begin{aligned}\alpha &= C_{11}n_1^2 + C_{66}n_2^2, \\ \beta &= C_{66}n_1^2 + C_{22}n_2^2, \\ \delta &= (C_{12} + C_{66})n_1n_2,\end{aligned}$$

for orthotropic materials and

$$\begin{aligned}\alpha &= C_{11}n_1^2 + C_{66}n_2^2, \\ \beta &= C_{66}n_1^2 + C_{11}n_2^2, \\ \delta &= (C_{12} + C_{66})n_1n_2,\end{aligned}$$

for cubic materials.

## B Material properties

Following we present the properties used along the paper.

### B.1 Two dimensions

- Aluminum:

$$[C] = \begin{bmatrix} 112.35 & 60.49 & 0 \\ 60.49 & 112.35 & 0 \\ 0 & 0 & 25.9 \end{bmatrix} \text{ GPa}, \quad \rho = 2700 \text{ kg/m}^3.$$

- GaAs:

$$[C] = \begin{bmatrix} 118.8 & 59.4 & 0 \\ 59.4 & 118.8 & 0 \\ 0 & 0 & 53.7 \end{bmatrix} \text{ GPa}, \quad \rho = 5320 \text{ kg/m}^3.$$

- Graphite:

$$[C] = \begin{bmatrix} 235 & 3.69 & 0 \\ 3.69 & 26 & 0 \\ 0 & 0 & 28.2 \end{bmatrix} \text{ GPa}, \quad \rho = 1790 \text{ kg/m}^3.$$

## B.2 Three dimensions

- Aluminum:

$$[C] = \begin{bmatrix} 112.35 & 60.49 & 60.49 & 0 & 0 & 0 \\ 60.49 & 112.35 & 60.49 & 0 & 0 & 0 \\ 60.49 & 60.49 & 112.35 & 0 & 0 & 0 \\ 0 & 0 & 0 & 25.9 & 0 & 0 \\ 0 & 0 & 0 & 0 & 25.9 & 0 \\ 0 & 0 & 0 & 0 & 0 & 25.9 \end{bmatrix} \text{ GPa}, \quad \rho = 2700 \text{ kg/m}^3.$$

- $\beta$ -brass:

$$[C] = \begin{bmatrix} 52 & 27.5 & 27.5 & 0 & 0 & 0 \\ 27.5 & 52 & 27.5 & 0 & 0 & 0 \\ 27.5 & 27.5 & 52 & 0 & 0 & 0 \\ 0 & 0 & 0 & 173 & 0 & 0 \\ 0 & 0 & 0 & 0 & 173 & 0 \\ 0 & 0 & 0 & 0 & 0 & 173 \end{bmatrix} \text{ GPa}, \quad \rho = 7600 \text{ kg/m}^3.$$

- Cadmium:

$$[C] = \begin{bmatrix} 115.9 & 41.05 & 41 & 0 & 0 & 0 \\ 41.05 & 115.9 & 41 & 0 & 0 & 0 \\ 41 & 41 & 51.2 & 0 & 0 & 0 \\ 0 & 0 & 0 & 19.95 & 0 & 0 \\ 0 & 0 & 0 & 0 & 19.95 & 0 \\ 0 & 0 & 0 & 0 & 0 & 37.43 \end{bmatrix} \text{ GPa}, \quad \rho = 8650 \text{ kg/m}^3.$$

- Carbon-Epoxy:

$$[C] = \begin{bmatrix} 12.37 & 6.15 & 6.19 & 0 & 0 & 0 \\ 6.15 & 21.37 & 6.19 & 0 & 0 & 0 \\ 6.19 & 6.19 & 146.30 & 0 & 0 & 0 \\ 0 & 0 & 0 & 4.80 & 0 & 0 \\ 0 & 0 & 0 & 0 & 4.80 & 0 \\ 0 & 0 & 0 & 0 & 0 & 3.11 \end{bmatrix} \text{ GPa}, \quad \rho = 1900 \text{ kg/m}^3.$$

## References

- George B. Arfken, Hans J. Weber, and Frank Harris. *Mathematical Methods for Physicists*. Academic Press, 6 edition, 2005.
- Bertram Alexander Auld. *Acoustic fields and waves in solids*, volume 1. Wiley New York, 1973.
- Biswajit Banerjee. *An Introduction to Metamaterials and Waves in Composites*. Taylor & Francis, 1 edition, 6 2011.
- Felix Bloch. Über die quantenmechanik der elektronen in kristallgittern. *Zeitschrift für physik*, 52(7-8):555–600, 1929.
- Léon Brillouin. *Wave propagation in periodic structures: electric filters and crystal lattices*. Courier Dover Publications, 2003.
- V. T. Buchwald. Elastic waves in anisotropic media. *Proceedings of the Royal Society of London. Series A. Mathematical and Physical Sciences*, 253(1275):563–580, 1959.
- José M. Carcione. *Wave fields in real media: Wave propagation in anisotropic, anelastic, porous and electromagnetic media*. Elsevier, 2007.
- F Casadei and JJ Rimoli. Anisotropy-induced broadband stress wave steering in periodic lattices. *International Journal of Solids and Structures*, 50 (9):1402–1414, 2013.
- Pierre A. Deymier. *Acoustic metamaterials and phononic crystals*, volume 173. Springer Science & Business Media, 2013.
- Benjamin M Goldsberry and Michael R Haberman. Negative stiffness honeycombs as tunable elastic metamaterials. *Journal of Applied Physics*, 123(9):091711, 2018.
- Nicolás Guarín-Zapata, Juan Gómez, David Kisailus, and Pablo D. Zavatieri. Bandgap tuning in bioinspired helicoidal composites. *Journal of the Mechanics and Physics of Solids*, 131:344–357, October 2019. ISSN 00225096. doi: 10.1016/j.jmps.2019.07.003. URL <https://linkinghub.elsevier.com/retrieve/pii/S0022509619302431>.
- Nicolás Guarín-Zapata, Juan Gomez, Camilo Valencia, Gary F. Dargush, and Ali Reza Hadjesfandiari. Finite element modeling of micropolar-based phononic crystals. *Wave Motion*, 92:102406, January 2020.

ISSN 01652125. doi: 10.1016/j.wavemoti.2019.102406. URL <https://linkinghub.elsevier.com/retrieve/pii/S0165212519300526>.

Mahmoud I. Hussein, Michael J. Leamy, and Massimo Ruzzene. Dynamics of phononic materials and structures: Historical origins, recent progress, and future outlook. *Applied Mechanics Reviews*, 66(4), 2014.

John Joannopoulos, Steven Johnson, Joshua Winn, and Robert Meade. *Photonic Crystals: Molding the Flow of Light*. Princeton University Press, 2 edition, 2008.

Steven G. Johnson. Notes on the algebraic structure of wave equations. Technical report, Massachusetts Institute of Technology, 2010.

Toufik Kanit, Franck N'Guyen, Samuel Forest, Dominique Jeulin, Matt Reed, and Scott Singleton. Apparent and effective physical properties of heterogeneous materials: Representativity of samples of two materials from food industry. *Computer Methods in Applied Mechanics and Engineering*, 195(33):3960–3982, 2006.

Charles Kittel. *Introduction to Solid State Physics*. Wiley, 7 edition, 1996.

Philippe Langlet. *Analyse de la propagation des ondes acoustiques dans les matériaux périodiques à l'aide de la méthode des éléments finis*. PhD thesis, Valenciennes, 1993.

Hassel Ledbetter and Albert Migliori. A general elastic-anisotropy measure. *Journal of applied physics*, 100(6):063516, 2006.

Florian Maurin, Claus Claeys, Elke Deckers, and Wim Desmet. Probability that a band-gap extremum is located on the irreducible Brillouin-zone contour for the 17 different plane crystallographic lattices. *International Journal of Solids and Structures*, 135:26–36, 2018. doi: 10.1016/j.ijsolstr.2017.11.006. URL <https://www.sciencedirect.com/science/article/pii/S0020768317305103>.

Jean-Claude Michel, Hervé Moulinec, and Pierre Suquet. Effective properties of composite materials with periodic microstructure: a computational approach. *Computer methods in applied mechanics and engineering*, 172(1-4):109–143, 1999.

Graeme W. Milton and Andrej V. Cherkaev. Which elasticity tensors are realizable? *Journal of Engineering Materials and Technology*, 1995.

- Maher Moakher and Andrew N. Norris. The closest elastic tensor of arbitrary symmetry to an elasticity tensor of lower symmetry. *Journal of Elasticity*, 85(3):215–263, 2006. doi: 10.1007/s10659-006-9082-0. URL <http://link.springer.com/article/10.1007/s10659-006-9082-0>.
- Andrew N Norris and Michael R Haberman. Introduction to the special issue on acoustic metamaterials. *The Journal of the Acoustical Society of America*, 132(4):2783–2783, 2012.
- Andrew N. Norris and Adam J. Nagy. Metal water: A metamaterial for acoustic cloaking. *Proceedings of Phononics, Santa Fe, New Mexico, USA*, pages 112–113, 2011.
- John Frederick Nye et al. *Physical properties of crystals: their representation by tensors and matrices*. Oxford university press, 1985.
- Yan Pennec, Jérôme O. Vasseur, Bahram Djafari-Rouhani, Leonard Dobrzański, and Pierre A. Deymier. Two-dimensional phononic crystals: Examples and applications. *Surface Science Reports*, 65(8):229–291, 2010.
- Shivakumar I. Ranganathan and Martin Ostoja-Starzewski. Universal elastic anisotropy index. *Physical Review Letters*, 101(5):055504, 2008.
- J.N. Reddy. *Applied Functional Analysis and Variational Methods in Engineering*. Krieger Publishing, 1 edition, 1991.
- M Ruzzene and F Scarpa. Directional and band-gap behavior of periodic auxetic lattices. *physica status solidi (b)*, 242(3):665–680, 2005.
- Massimo Ruzzene, Fabrizio Scarpa, and Francesco Soranna. Wave beam-ing effects in two-dimensional cellular structures. *Smart materials and structures*, 12(3):363, 2003.
- Nico Schrömer. meshzoo. <https://github.com/nschloe/meshzoo>, 2020.
- Anthony Scopatz and Kathryn D. Huff. *Effective computation in physics: Field guide to research with Python*. O'Reilly Media, Inc., 2015. URL <http://physics.codes/>.
- M. M. Sigalas and Nicolas Garcia. Theoretical study of three dimensional elastic band gaps with the finite-difference time-domain method. *Journal of Applied Physics*, 87(6):3122–3125, 2000.
- N. Sukumar and J. E. Pask. Classical and enriched Finite element formulations for Bloch-periodic boundary conditions. *International Journal of Numerical Methods in Engineering*, 77(8):1121–1138, 2 2009.

Leon Thomsen. Weak elastic anisotropy. *Geophysics*, 51(10):1954–1966, 1986.

Camilo Valencia, Juan Gomez, and Nicolás Guarín-Zapata. A General-Purpose Element-Based Approach to Compute Dispersion Relations in Periodic Materials with Existing Finite Element Codes. *Journal of Theoretical and Computational Acoustics*, page 1950005, July 2019a. ISSN 2591-7285, 2591-7811. doi: 10.1142/S2591728519500051. URL <https://www.worldscientific.com/doi/abs/10.1142/S2591728519500051>.

Camilo Valencia, David Restrepo, Nilesh D Mankame, Pablo D Zavattieri, and Juan Gomez. Computational characterization of the wave propagation behavior of multi-stable periodic cellular materials. *Extreme Mechanics Letters*, 33:100565, 2019b.

Pauli Virtanen, Ralf Gommers, Travis E. Oliphant, Matt Haberland, Tyler Reddy, David Cournapeau, Evgeni Burovski, Pearu Peterson, Warren Weckesser, Jonathan Bright, et al. SciPy 1.0: fundamental algorithms for scientific computing in Python. *Nature methods*, 17(3):261–272, 2020.

John R Willis. Negative refraction in a laminate. *Journal of the Mechanics and Physics of Solids*, 97:10–18, 2016.

Clarence Zener. *Elasticity and anelasticity of metals*. University of Chicago press, 1948.

Xiangdong Zhang and Zhengyou Liu. Negative refraction of acoustic waves in two-dimensional phononic crystals. *Applied Physics Letters*, 85(2):341–343, 2004.